Mikada, H., Becker, K., Moore, J.C., Klaus, A., et al., 2002
Proceedings of the Ocean Drilling Program, Initial Reports Volume 196

1. Leg 196 Summary: Deformation and Fluid Flow Processes in the Nankai Trough Accretionary Prism: Logging While Drilling and Advanced CORKs[1]

Shipboard Scientific Party[2]

ABSTRACT

Leg 196 was the second of a two-leg program of coring, logging, and installing Advanced CORK (ACORK) long-term hydrogeological observatories in the Nankai Trough, the type example of a convergent margin accreting a thick section of clastic sediments. The two-leg program (Legs 190 and 196) was built on results from Leg 131 and was designed to define the interrelationship of deformation, structure, and hydrogeology in the Nankai accretionary prism. Leg 196 focused on logging while drilling (LWD) and installation of ACORKs at two sites near the toe of the Nankai prism: Site 808, cored during Leg 131 at the deformation front, and Site 1173, cored during Leg 190 as a reference site ~12 km seaward.

At Hole 1173B we collected LWD data to basement at 737 meters below seafloor (mbsf). Here the LWD data verify a subtle porosity increase with depth from 122 to 340 mbsf, followed downhole by a sharp decrease in porosity and return to a normal consolidation trend. The sharp decrease in porosity correlated with the diagenetic transition from cristobalite to quartz and is marked by a strong seismic reflector that is reproduced well by a synthetic seismogram based on the LWD data. In Hole, 1173B, resistivity-at-the bit (RAB) images of the borehole show no evidence of a propagating protodécollement but, rather, reveal a basinal state of stress dominated by steeply dipping fractures and normal faults of variable strike.

[1]Examples of how to reference the whole or part of this volume.
[2]Shipboard Scientific Party addresses.

Ms 196IR-101

In Hole 808I we acquired LWD data to just below the décollement zone (1035 mbsf), where poor drilling conditions precluded further penetration. Here RAB images provide unparalleled structural and stratigraphic detail across the frontal thrust and décollement zones that indicate northwest-southeast shortening consistent with the seismic reflection data. RAB images also document borehole breakouts that show a northwest-southeast oriented maximum principal in situ stress direction, nearly parallel to the maximum principal stress direction inferred from microfaults in cores and from the plate convergence direction. Resistivity curves suggest that the frontal thrust zone has compacted, presumably due to shearing. In contrast, the resistivity data suggest that the décollement zone is dilated. These resistivity anomalies in the frontal thrust and décollement zones cannot be explained by variations in pore water composition and need to be verified by the density and porosity logs after careful correction for borehole washouts.

In Hole 1173B, a four-packer, five-screen ACORK installation was successfully emplaced. It was configured for monitoring the hydrogeological state and processes in basement and the stratigraphic projection of the décollement zone in the lower Shikoku Basin deposits. The ACORK in Hole 808I was configured with two packers and six screens and was intended to penetrate just to the décollement zone, with an emphasis on determining the hydrogeological state and processes at the frontal thrust zone, a fractured zone ~160 m below the frontal thrust, and the décollement zone. Owing to extreme deterioration of drilling conditions and underreamer failure, actual penetration concluded ~36 m short of the goal, but the ACORK remains a viable installation.

INTRODUCTION

Subduction zones are characterized by the world's largest and potentially most catastrophic earthquakes (Kanamori, 1986). Moreover, these plate convergence zones return materials to the Earth's interior with chemical fluxes that may impact global geochemical budgets and influence climate (Plank et al., 1998). Subduction zones also are the location of the incipient stages of formation of convergent and collisional mountain belts (Moores and Twiss, 1995).

Recent studies of the processes occurring at subduction zones have established beyond doubt that fluids play a major role in the physical and chemical evolution of subduction zones and mountain belts (e.g., Carson et al., 1990; Henry et al., 1989; Kastner et al., 1991; Vrolijk et al., 1991; Fisher, 1996). When sediments resting on the incoming or subducting plate meet the overriding plate, they are, in part, scraped off and deformed and, in part, underthrust. During this deformation and burial, tectonic stresses lead to the expulsion of intergranular fluids through compaction (Bray and Karig, 1985), increased temperatures cause mineral dehydration (Moore and Vrolijk, 1992), and biological and thermal processes produce hydrocarbons from organic matter (Suess and Whiticar, 1989). To understand the processes of fluid production, transport, and rock response requires not only detailed spatial and subsurface sampling but also long-term observations in the subseafloor. Accordingly, Ocean Drilling Program (ODP) Leg 196 was designed to measure the in situ physical properties and provide long-term monitoring of the physical and chemical states of the initial deformation zone of the subduction zone off of southwest Japan.

Evaluation of this solid and fluid flow in the subduction system off southwest Japan involves outstanding questions that can be addressed by our logging and monitoring program in combination with the borehole coring results from Legs 131 (Hill, Taira, Firth, et al., 1993) and 190 (Moore, Taira, Klaus, et al., 2001). These questions include

1. What is the character of the faulted rock and associated fluids of the plate-boundary thrust fault, or décollement?
2. What is the porosity or fluid content of the incoming sediments, the accretionary prism, and underthrust sediments?
3. What is the relationship between porosity and seismic velocity?
4. How and why does pore pressure vary between structural environments?
5. What changes in physical properties (especially velocity) occur in association with diagenetic alterations of sediments (particularly methane hydrate occurrence)?
6. What is the relationship between deformational structures at core, log, and seismic scales, and what do they tell us about tectonic processes in the accretionary prism?

Addressing these questions will provide a clearer understanding of the issues of deformation and fluid flow during shallow subduction and the basis for predicting the behavior of these materials at seismogenic depths.

GEOLOGICAL AND GEOPHYSICAL SETTING

The Nankai subduction zone off of southwest Japan forms an "end-member" sediment-dominated accretionary prism. Here, a sedimentary section ~1 km thick (Figs. **F1, F2**) is accreted to or underthrust beneath the margin in the style of a fold and thrust belt (Moore et al., 2001). The Philippine Sea plate underthrusts the margin at a rate of ~4 cm/yr along an azimuth of 310°–315° (Seno et al., 1993) down an interface dipping 3°–7° (Kodaira et al., 2000), causing repeated great earthquakes (magnitudes >8) with an average recurrence interval of ~180 yr (Ando, 1975). Currently the margin is locked with little convergence between the Muroto Peninsula and the Philippine Sea plate (Mazzotti et al., 2000). The convergent margin of southwest Japan has a geologic record of accretion of deep-sea deposits extending to at least the Cretaceous (Taira et al., 1988). However, rocks cored during Leg 190 (Fig. **F2**) and even those subducted to seismogenic depths entered the subduction zone no earlier than the Pliocene (Moore, Taira, Klaus, et al., 2001).

In the area of Leg 190/196 drilling, the Muroto Transect (Fig. **F1**), the basin to margin transition can be divided into the undeformed Shikoku Basin and overlying trench fill, the protothrust zone, the imbricate thrust zone, the frontal out-of-sequence thrust zone, the large thrust slice zone, and the landward-dipping reflector zone (Fig. **F2**). A condensed summary of these tectonic provinces from Moore et al. (2001) and Moore, Taira, Klaus, et al. (2001) follows.

The Philippine Sea plate entering the Nankai Trough along the Muroto Transect is near the axis of an extinct spreading center marked by the Kinan Seamounts (Okino et al., 1999). As documented at Site 1173, the 16-Ma oceanic crust of the Shikoku Basin is overlain by, successively, volcaniclastics, a middle Miocene to mid-Pliocene massive hemipelagite, an upper Pliocene to lower Pleistocene hemipelagite with

F1. Map of Leg 190 and 196 sites, p. 17.

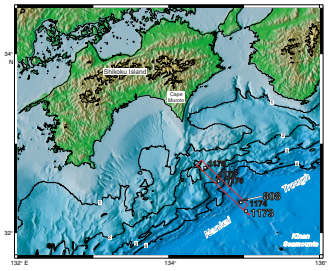

F2. Depth section of sites and structural features, p. 18.

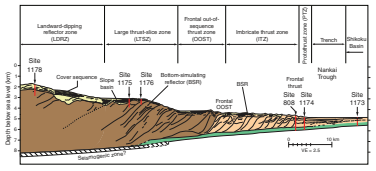

tephra layers, and a Pleistocene turbidite to hemipelagite transition sequence and a Pleistocene to Holocene trench turbidite unit.

Entering the protothrust zone, the ~1-km-thick sedimentary section initially deforms above a protodécollement zone or incipient detachment surface developed in the uppermost Miocene massive hemipelagite layer. The lower portion of this massive hemipelagite is underthrust beneath the accretionary prism along with underlying volcaniclastics and oceanic crust. Coring and seismic studies demonstrate that this initial deformation above the décollement zone consists of small thrust faults associated with subtle folding at seismic scales (Park et al., 2000) and development of minor faults at core scale (Moore, Taira, Klaus, et al., 2001; Morgan and Karig, 1995).

Major thrust faulting and growth of the accretionary prism initiate at the frontal thrust and continue upslope (Fig. F2). Immediately landward of the frontal thrust, the imbricate thrust zone consists of a series of well-developed seaward-vergent imbricate packets spaced several kilometers apart. The imbricate thrust zone is ~20 km wide; Site 808 penetrates its frontal thrust. Out-of-sequence thrusts overprint the imbricate thrusts, starting ~20 km landward of the deformation front. Farther landward from the deformation front, out-of-sequence thrusts cutting thick thrust packages define the large thrust slice zone. These out-of-sequence thrusts were probably initially imbricated from thick turbidite sands of the Shikoku Basin (Moore, Taira, Klaus, et al., 2001). The landward-dipping reflector zone upslope from the large thrust slice zone is less well imaged than more seaward portions of the prism. However, the landward-dipping reflectors probably represent thrust boundaries and in some cases tilted sedimentary layering.

The Leg 190/196 drilling area shows high heat flow (Wang et al., 1995) because the Muroto Transect is located near the extension of a ridge on the Philippine Sea plate (represented by the Kinan Seamounts) that ceased spreading at only 15 Ma. Conductive heat flow values range from 180 mW/m^2 at Sites 1173 and 1174 (Shipboard Scientific Party, 2001a, 2001b) to 130 mW/m^2 at Site 808 (Shipboard Scientific Party, 1991). Heat flow values decrease rapidly upslope from the Nankai Trough, verifying the anomalously warm nature of the trench area (Yamano et al., 1992). The simple extrapolation of conductive heat flow with depth may overestimate temperature because of the potential of heat advection associated with fluid expulsion from the deforming sedimentary sequence. The temperatures at the top of oceanic crust at Sites 1173 and 808 were estimated at 110° and 120°C, respectively, by a conductive extrapolation of shallower measurements (Shipboard Scientific Party, 1991, 2001a). A less reliable extrapolation of only two very shallow data points at Site 1174 suggests a comparable basement temperature there (Shipboard Scientific Party, 2001b). Thus, the evidence indicates that basement temperatures exceed 100°C at Sites 1173, 1174, and 808. These high temperatures drive diagenetic reactions that significantly influence log response.

FLUID FLOW INDICATORS AND LEG 196 OBJECTIVES

Geochemical measurements may indicate lateral fluid flow through the sediments in the Leg 196 area, although its presence and magnitude is controversial. Specifically the evidence of décollement zone–hosted

fluid flow is equivocal (Shipboard Scientific Party, 1991; Kastner et al., 1993). Landward of the deformation front, the décollement zone steps down through a water-rich massive hemipelagite below, suggesting that the décollement zone could be progressively dewatering there, with the fluid possibly being expelled seaward up the décollement zone (Park et al., 2000). The broad minimum in the pore water chloride profile obtained during Legs 131 and 190 at Sites 808 and 1174, extending from right above to well below the décollement zone, was probably produced by a combination of in situ clay dehydration and vertical fluid migration, possibly with a component of lateral migration (Kastner et al., 1993; Shipboard Scientific Party, 2001b).

Although the role of fluid is thought to be a key in the study of seismogenic zones (Hickman et al., 1995). The magnitude and location of active fluid flow in this accretionary prism and the potential linkage to the Nankai seismogenic zone are not clearly defined. Our desire to investigate this system motivated the deployment of long-term hydrogeological and geochemical monitoring systems or Advanced CORKs (ACORKs) during Leg 196. By sampling particular stratigraphic and structural intervals, the ACORKs will constrain fluid pressures and permeability and provide a time series of the fluid flow regime at the toe of the Nankai accretionary prism. Thus, our results may provide a better understanding of the linkage of near-surface conditions to those in the seismogenic zone, especially in the case of an earthquake rupturing the deeper levels of the décollement zone.

SITE SUMMARIES

Site 1173

We drilled Holes 1173B and 1173C (Table T1) to obtain logging-while-drilling (LWD) data at a reference site on the seaward flank of the Nankai Trough and to install an ACORK long-term subseafloor hydrological monitoring experiment (Figs. F1, F2, F3, F4, F5, F6). These holes complement Hole 1173A, which was cored from the surface to basement during Leg 190. This site provides a basis for comparison of physical and chemical properties between the incoming undeformed sediments and rocks of the Shikoku Basin with deformed materials of the accretionary prism and underthrust sediments cored at sites landward of the deformation front.

Log Quality

At Site 1173, the LWD tools measured resistivity at the bit (RAB), sonic velocity, density, porosity, natural gamma ray production, and photoelectric effect from the seafloor to basaltic basement. Additionally, the tools provided estimates of hole size and borehole resistivity images. A measurement-while-drilling system supplied information on weight on bit, torque, heave, resistivity, density, and sonic velocity that was communicated to the surface and displayed instantaneously during drilling.

The overall quality of the LWD logs recorded in Holes 1173B and 1173C is excellent. The LWD logs generally confirm the more limited Hole 1173A wireline logs. In Holes 1173B and 1173C the drilling rate was maintained between 35 and 60 m/hr throughout the section, and all measurements were made within 1 hr of bit penetration. At least two

T1. Operations summary, p. 28.

F3. Seismic time section across Sites 1173 and 808, p. 19.

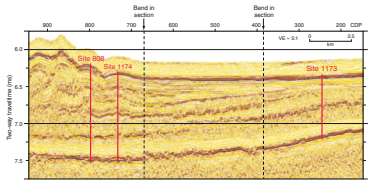

F4. Seismic depth section across Sites 1173, 1174, and 808, p. 20.

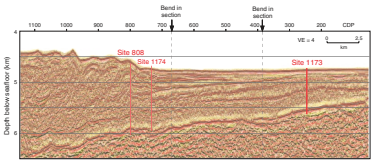

F5. Composite seismic section through Leg 196 drill sites, p. 21.

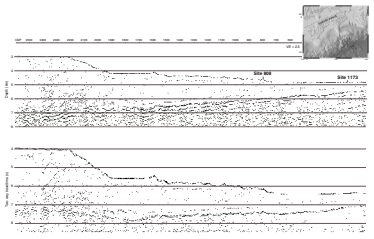

F6. Site 1173 seismic, lithologic, and logging summary, p. 22.

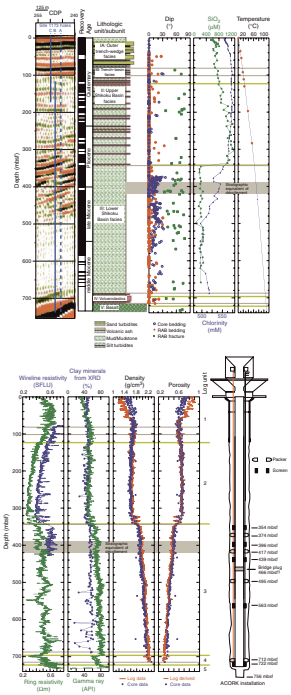

depth points were measured in each 0.30-m interval. The caliper shows that the gap between the bit radius and the hole is <1 in throughout both holes, except for the uppermost 75 m of Hole 1173C, where soft sediment washed out a gap of up to 2 in. Therefore, the density log over this shallowest 75-m interval is unreliable. This was the first use of the LWD Integrated Drilling Evaluation and Logging (IDEAL) sonic-while-drilling (ISONIC) velocity tool in such fine-grained unlithified sediment and its first use by ODP. Although the tool worked well, the processing of the waveforms was not straightforward and will have to be improved postcruise to yield reliable sonic velocity data.

Log Units and Lithology

Both visual and multivariate statistical analyses of the logs define five log units that account for the lithologic variations observed in the cores.

A high variability in the differential caliper log and a large number of caliper values >1 in reflect bad borehole conditions during drilling of the upper 75 m of log Unit 1 (0–122 meters below seafloor [mbsf]). This log unit shows high neutron porosity and low density values with a high standard deviation. Some of these variations might be real and reflect silt and sand turbidites of the outer trench–wedge facies. A significant decrease of resistivity, density, and gamma ray and increase of neutron porosity with depth show an abnormal compaction trend and define log Unit 2 (122–340 mbsf). This log unit correlates with lithologic Unit II (102–344 mbsf), which consists of hemipelagic mud with abundant interbeds of volcanic ash. The low density could be related to a cementation effect due to the formation of cristobalite. The log Unit 2/3 boundary correlates with the diagenetic phase transition between cristobalite and quartz. High gamma ray, density, and photoelectric effect log values that increase continuously with depth characterize log Unit 3 (340–698 mbsf). Resistivity and, less obviously, gamma ray logs show a cyclicity (480–700 mbsf) that reflects changes in lithology, which may in turn reflect an interbedding of coarser and finer grained sediments. Log Unit 4 (698–731 mbsf) is defined by broad variations in photoelectric effect, resistivity, neutron porosity, and gamma ray logs that correlate well with the presence of the volcaniclastic facies of lithologic Unit IV (688–724 mbsf). Log Unit 5 (731–735 mbsf) shows an abrupt increase of resistivity and decrease of gamma ray, log values which characterize the basaltic oceanic basement.

Structural Geology

Structural data determined from RAB images of medium-focused resistivity (penetration depth = 7.6 cm beyond the standard borehole radius) indicate sparse deformation and predominantly subhorizontal bedding dips. Increases in bedding dips (5°–35°) at 50–200 mbsf and below ~370 mbsf agree with core data from Leg 190 Hole 1173A. Fractures are high angle (40°–80°), show normal displacement where measurable, and have variable strike orientation. Resistive fractures dominate and might reflect nonconductive clay gouge, mineralization, or porosity collapse due to compaction. An increase in fracture intensity occurs at 380–520 mbsf, correlating with increased bedding dip. The upper limit of this zone corresponds to the stratigraphic equivalent of the décollement zone. At ~500 mbsf, bands of heterogeneous (mottled) high resistivity probably represent zones of intense deformation or brecciation.

In general, deformation observed in Holes 1173B and 1173C is consistent with extensional faulting probably related to basinal compaction and burial and not to propagating compressional deformation from the accretionary wedge.

Physical Properties

LWD density data in Holes 1173B and 1173C closely match core physical properties data from Hole 1173A, except for the uppermost 60 m, where the differential caliper exceeded 1 in. LWD densities are nearly constant in log Subunit 1b (55–122 mbsf) and Unit 2 (122–340 mbsf), with the notable exceptions of two high-amplitude variations near the transition from lithologic Unit II (upper Shikoku Basin) to III (lower Shikoku Basin). Log Unit 3 (340–698 mbsf) is characterized by a steady increase in density consistent with normal compaction. The LWD resistivity logs clearly respond to the lithologic boundaries identified in Hole 1173A. Within log Unit 2 resistivity decreases with depth while density is constant, whereas in log Unit 3, resistivity is nearly constant with depth while density increases. All LWD resistivity logs show a similar overall trend, in good agreement with available wireline logs. Shallow-focused button resistivities that are consistently higher than medium and deep resistivities are unusual and an unexplained feature of Site 1173 LWD data.

Logs and Seismic Reflection Data

The velocities from the core and wireline data and densities from the core and LWD data from 0 to 350 mbsf were used to generate a synthetic seismogram in good agreement with the seismic reflection data. Good correlations exist between the synthetic seismogram and seismic reflections at ~80–100 (trench–basin transition facies), ~175, ~265–270, and ~300–350 mbsf (associated with the upper/lower Shikoku Basin unit boundary and the log Unit 2/3 boundary). An increase in acoustic impedance associated with the phase transition from cristobalite to quartz may be, in part, responsible for this reflection. High reflectivity in the synthetic seismogram beneath ~350 mbsf does not match with the low reflectivity in the seismic data of the lower Shikoku Basin unit (log Unit 3) and may be due to a sampling bias toward more cohesive, higher velocity samples in the core velocity measurements.

ACORK Installation and Basement Coring

A four-packer, five-screen, 728-m-long ACORK string (Fig. F6) was deployed through the sediment section in Hole 1173B, configured to emphasize long-term observations of pressures in three principal zones, as follows:

1. Oceanic basement below 731 mbsf, to determine permeability and pressures in the young oceanic crust being subducted and thereby assess the role of oceanic crust in the overall hydrogeology of the Nankai Trough. A screen was installed immediately above the ACORK shoe, centered at 722 mbsf, and a packer was placed immediately above the screen.
2. Lowermost Shikoku Basin deposits, well below the stratigraphic projection of the décollement zone, to assess the hydrological properties of a reference section of the lower Shikoku Basin de-

posits and test for fluid pressure propagation from basement or possibly higher in the section. A packer was centered at 495 mbsf to isolate a screen centered at 563 mbsf.

3. The stratigraphic equivalent of the décollement zone at ~390–420 mbsf in the upper part of the lower Shikoku Basin deposits seaward from Sites 1174 and 808. A symmetric array, ~100 m long, comprising three screens separated by two packers, was built into the ACORK string so that the screens were centered at 439, 396, and 353 mbsf. Objectives of this array include (1) documenting the variation of hydrogeological properties across and away from this zone as a reference for the state of the formation before the décollement zone actually develops closer to the trench axis and (2) detecting the possibility of elevated fluid pressure or fluid flow along the stratigraphic projection of the décollement zone. In addition, the central screen in this array (the screened interval that spans the stratigraphic equivalent of the décollement zone) includes a second small-diameter line for eventual sampling of formation fluids from the well head.

After ACORK installation, the rotary core barrel coring bottom-hole assembly was successfully deployed through the ACORK casing (Fig. **F34,** p. 72, in the "Site 1173" chapter) to deepen the hole into basement to assure that the signal of basement hydrogeological processes will be transmitted to the deepest screen. A total of 19.5 m into basement was cored, with recovery of 5.2 m (27% recovery). The core comprises basaltic basement overlain by a thin veneer of volcaniclastics.

Following the basement coring, the final step in the ACORK installation at Hole 1173B was deployment of a bridge plug to seal the bore of the casing and isolate the basement section to be monitored by the deepest screen. We intended to set the bridge plug very near the bottom of the ACORK string, allowing future deployment of other sensor strings within the central bore. However, the bridge plug apparently set prematurely at 466 mbsf; this was not sensed at the rig floor and ensuing operations resulted in breaking the pipe off at the ACORK head. Nevertheless, detailed analysis suggests that the bridge plug is indeed set, and a video inspection confirmed that there is no broken pipe outside the ACORK head to inhibit future data recovery operations (Fig. **F35,** p. 73, in the "Site 1173" chapter).

F7. Site 808 seismic, lithologic, and logging summary, p. 24.

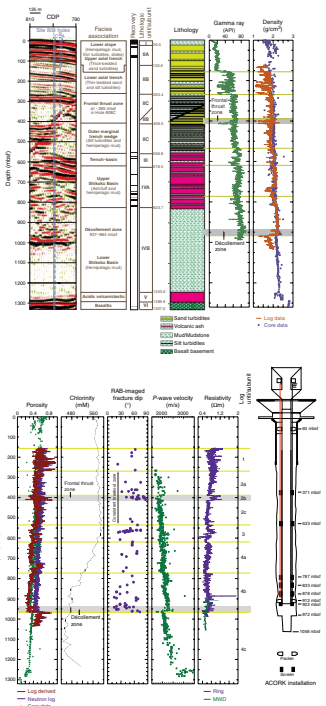

Site 808

We drilled Hole 808I (Table **T1**) to obtain LWD data through the frontal thrust and décollement zones at the deformation front of the Nankai Trough and to install an ACORK long-term subseafloor hydrological monitoring experiment (Figs. **F5, F7**). This hole complements cores recovered at Site 808 during Leg 131. Coring, logging, and monitoring here are intended to document the physical and chemical state of the Nankai accretionary prism and underthrust sediments through the frontal thrust zone, the décollement zone, and into oceanic basement.

Log Quality

The overall quality of the LWD logs recorded in Hole 808I is variable. We recorded at least one sample per 15 cm over 99% of the total section. Sections of enlarged borehole estimated by the differential caliper

yield unreliable density data and associated derived porosity that is confirmed by comparison to core data. This problem is primarily associated with the depth intervals 725–776 and 967–1057 mbsf, in which there was a long duration between drilling and recording of the logs due to wiper trips or poor hole conditions. Density and density-derived porosity should be used cautiously until more complete corrections and editing are completed postcruise. Although the LWD ISONIC tool worked well, the processing of the waveforms was not straightforward and postcruise processing is required to yield reliable sonic data.

Log Units and Lithology

A combination of visual interpretation and multivariate statistical analysis defined four log units and six log subunits.

Log Unit 1 (156–268 mbsf) is characterized by the overall lowest mean values of gamma ray, density, and photoelectric effect and overall highest mean values of resistivity and neutron porosity. These values coincide with very fine grained sandstone, siltstone, and clayey siltstone/silty claystone observed in the cores. Log Unit 2 (268–530 mbsf) shows a constant value range of gamma ray and neutron porosity and a decreasing resistivity log. A high variability in the differential caliper log and a large number of values >1 in reflect poor borehole conditions. Log Unit 3 (530–620 mbsf) is marked by a significant increase in mean values of gamma ray, density, and photoelectric effect logs. Log Unit 4 (620–1035 mbsf) is characterized by the overall highest mean values of gamma ray, photoelectric effect, and density and the lowest mean values of resistivity and neutron porosity. Generally, a positive correlation between gamma ray and photoelectric effect is observed. A continuous increase in gamma ray and photoelectric effect, which reflects an increase in clay and carbonate content, is observed from log Unit 1 to log Unit 4. A positive correlation between resistivity with density defines log Units 3 and 4.

Structural Geology

RAB tools imaged fracture populations and borehole breakouts throughout much of the borehole. We identified both resistive and conductive fractures, respectively interpreted as compactively deformed fractures (leading to porosity collapse) and open fractures. Fractures are concentrated in discrete deformation zones that correlate with core analysis performed during Leg 131: the frontal thrust zone (389–414 mbsf), a fractured interval (559–574 mbsf), and the décollement zone (~940–960 mbsf). Only relatively sparse deformation occurs between these zones. The major deformation zones are characterized by conductive fractures and overall high resistivity, with resistive fractures between these zones. Fractures are steeply dipping (majority >30°) and strike predominantly east-northeast–west-southwest, close to perpendicular to the convergence vector (~310°–315°; Seno et al., 1993). Bedding dips are predominantly low angle (<50°) but are difficult to identify in the highly deformed zones, therefore biasing this result. Bedding strike is more random than fracture orientation, but, where a preferred orientation is recorded, beds strike subparallel to fractures and approximately perpendicular to the convergence vector.

The frontal thrust zone (389–414 mbsf) represents the most highly deformed zone in Hole 808I and contains predominantly south-dipping fractures (antithetic to the seismically imaged main thrust

fault) and a few north-dipping east-northeast–west-southwest striking fractures. The highly fractured interval at 559–574 mbsf contains similar fracture patterns to the frontal thrust zone. Both deformation zones are characterized by high-conductivity (open?) fractures within a zone of overall high resistivity.

Deformation at the décollement zone is more subdued and is represented by a series of discrete fracture zones. The décollement zone in the RAB images (937–965 mbsf) is defined by a general increase in fracture density and variability in physical properties.

Borehole breakouts are recorded throughout Hole 808I and are particularly strongly developed within log Unit 2 (270–530 mbsf), suggesting lithologic control on sediment strength and breakout formation. Breakouts indicate a northeast-southwest orientation for the minimum horizontal compressive stress (σ_2), consistent with a northwest-southeast convergence vector (~310°–315°, parallel to σ_1; Seno et al., 1993). Breakout orientation deviates slightly from the dominant strike of fractures (east-northeast–west-southwest), but this deviation may be within error of measurements.

Physical Properties

The Hole 808I LWD density log shows a good fit to the core bulk density, slightly underestimating core values in the upper 550 mbsf and slightly overestimating core values between 550 and 970 mbsf. Below 156 mbsf the LWD density log shows a steady increase from ~1.7 to ~1.95 g/cm^3 at 389 mbsf. Between 389 and 415 mbsf density varies greatly, corresponding to the frontal thrust zone. The low density values here are probably spurious, produced by washout of the borehole. Below the frontal thrust zone density decreases sharply to ~1.85 g/cm^3. Below 530 mbsf it increases to ~2.1 g/cm^3. Between 725 and 776 mbsf density drops sharply to ~1.75 g/cm^3, corresponding to a period of borehole wiper trips. Density increases more rapidly from ~1.95 g/cm^3 at 776 mbsf to 2.25 g/cm^3 at 930 mbsf, decreasing steadily to ~2.15 g/cm^3 before stepping down to 1.4 g/cm^3 at 965 mbsf. This corresponds to the base of the décollement zone; below, density increases steadily from ~1.7 g/cm^3 at 975 mbsf to ~2.0 g/cm^3 at 1034.79 mbsf.

The downhole variation of LWD resistivity measurements shows identical trends in all five resistivity logs of Hole 808I. All log unit boundaries are clearly identified. Log Unit 1 has an average resistivity of 0.8–0.9 Ωm. After a sharp decrease in resistivity from 1.3 to 0.5 Ωm between 156 and 168 mbsf, the signal shows an increasing trend downward to the boundary between log Units 1 and 2. Log Unit 2 is characterized by an overall decreasing trend in resistivity from ~0.9 to ~0.6 Ωm. However, this trend is sharply offset from 389 to 415 mbsf (log Subunit 2b), where resistivity values are ~0.3 Ωm higher. This zone seems to correspond to the frontal thrust; the higher resistivity here may reflect compactive deformation in the frontal thrust zone. Log Unit 3 shows a higher degree in variability of the resistivity signal. Resistivity exhibits less variation again in log Unit 4, where it averages ~0.6 Ωm. At ~925 mbsf resistivity changes trend from a gradual increase to a gradual decrease. This decreasing trend persists to the base of the décollement zone at ~960 mbsf. As observed in Hole 1173B, shallow-focused resistivity is systematically higher than both medium and deep resistivity.

Logs and Seismic Reflection Data

Beneath the casing (~150 mbsf), correlations between the synthetic seismogram and seismic reflection data are only broadly consistent. The details of amplitude and waveform throughout most of the section do not match the seismic data. Amplitudes of the intervals between ~200 and ~400 mbsf, between ~750 and ~850 mbsf, and below ~925 mbsf are significantly higher in the synthetic seismogram than in the seismic data and are probably generated by numerous anomalously low velocity and density values. The seismic data cannot be matched with the synthetic seismograms produced from the logs because of the large variations in velocity and density. These results and the poor hole conditions raise doubts about the validity of portions of these logs.

ACORK Installation

In Hole 808I we assembled a 964-m-long ACORK casing string incorporating two packers and six screens for long-term observations of pressures in three principal zones, as follows:

1. The décollement zone and overlying section of the lower Shikoku Basin deposits (lithologic Unit IV). A screen was placed immediately above the casing shoe, with a packer immediately above the screen. The hole was opened with the intent of emplacing the screen just into the décollement zone, with the packer positioned in a competent section immediately above the décollement zone. Three other screens were configured above the packer, to span the upper section of the lower Shikoku Basin deposits to study the variation of physical properties and the propagation of any pressure signals away from the décollement zone.
2. A fractured interval at 560–574 mbsf in the upper Shikoku Basin deposits, as identified in RAB logs (see **"560-mbsf Fractured Interval,"** p. 21, in "Logs and Structural Geology" in the "Site 808" chapter). A single screen was intended to be deployed in this zone.
3. The frontal thrust zone, centered at ~400 mbsf. A single screen was intended to be deployed in this zone.

Drilling conditions during installation of the ACORK steadily worsened, starting ~200 m above the intended total depth. Despite all efforts, progress stopped 37 m short of the intended installation depth. This left the screen sections offset above the intended zones (Fig. **F7**), not an ideal installation but still viable in terms of scientific objectives. In addition, this left the ACORK head 42 m above the seafloor, unable to support its own weight once we pulled the drilling pipe out (Fig. **F31,** p. 64, in the "Site 808" chapter). Fortunately, when the ACORK head fell over, it landed on the seafloor such that all critical components remained in good condition (Fig. **F32,** p. 65, in the "Site 808" chapter). This includes the critical hydraulic umbilical, data logger, and the underwater-mateable connector, which remains easily accessible by a remotely operated vehicle or by submersible for data download.

TOPICAL HIGHLIGHTS AND QUESTIONS

Borehole Images, Structural Characterization, Breakouts, Stress Orientations, and Stress Magnitudes

Imaging of the borehole by RAB provided one of the immediate products of Leg 196 (Figs. F8, F9). The RAB images provide an in situ view of borehole structure unparalleled in completeness, although at a lower resolution than the cores. Nevertheless, combining these images with information on core structures provides probably the best view so far of the initial deformation in a subduction zone. At Site 1173 we imaged steeply dipping normal faults and fractures of variable strikes, which would be expected from the state of stress in a consolidating sedimentary basin. Conversely, the fractures are more consistent in dip azimuth in Hole 808I (Fig. F8), suggesting the influence of compressional deformation in the frontal thrust zone. One of the most spectacular results of Leg 196 is imaging the breakouts in Hole 808I and their definition of a principal stress orientation parallel to that determined by the inversion of small faults (Lallemant et al., 1993) and parallel to that expected from the convergence vector (Seno et al., 1993). These breakouts are concentrated in log Unit 2 at Site 808. Additional analysis of breakout orientation, width, and depth along with determination of the cohesion and coefficient of friction of the sedimentary rocks should provide a better resolution of stress orientation as well as stress magnitude.

F8. RAB image showing interpreted fractures, p. 26.

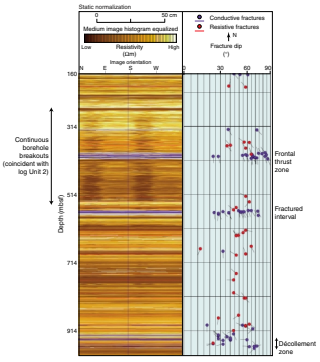

F9. Breakouts from shallow, medium, and deep RAB images, p. 27.

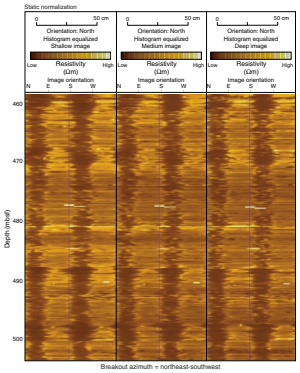

Contrasting Log Response across Faults and Predictions of Fluid Pressure

Tectonic consolidation of sediment in fault zones is influenced by fluid pressure. Thus, depth profiles of density or porosity variation through fault zones provide an overall view of fault zone behavior and a qualitative predictor of fluid pressure. From Hole 808I, we collected log data through the frontal thrust and décollement zones. This information, combined with existing core-scale density and porosity information, provides a unique view of major fault dynamics.

The density and density-derived porosity logs are suspect in the frontal thrust and décollement zones because of enlarged hole diameter. However, resistivity data provide insights on porosity variation. For example, the frontal thrust zone shows a sharp and sustained increase in resistivity. Because the pore water shows no significant variations in composition through this zone, it is unlikely that the resistivity increase is caused by differing fluid composition. Rather, the increase in resistivity may indicate a densification of the rock unit due to compaction accompanying shear.

At the top of the décollement zone, the resistivity trend changes from gradually increasing to gradually decreasing. The pore water chemistry around the décollement zone shows no anomalies that would explain the decreasing resistivity. The decreasing resistivity trend is presumably a response to the increased amount of fluid-filled unhealed fractures and a bulk porosity increase. In contrast, core porosity decreases in the décollement zone. Therefore, a combination of log and core measurements suggests that the décollement is an interval of enhanced porosity (probably fracture porosity) that encompasses blocks of sediment of relatively lower porosity and high density. Thus, the log data suggest that the fracture porosity of the décollement zone is di-

lated, probably held open by high fluid pressure, in contrast to the frontal thrust zone that is densified and may not be currently as highly overpressured.

The interpretations of fault zone porosity based on qualitative interpretation of resistivity must be verified by calculation of resistivity-derived porosity and appropriate corrections to the density data so that they can be utilized to calculate porosity. Additionally, direct fluid pressure measurements from the ACORK installation may provide information on fault zone pore pressures.

Porosity Changes, Silica Diagenesis, Reflectors, and the Décollement Zone

At Site 1173 density and porosity change downsection atypically for a normally consolidating sedimentary basin (Fig. F6). After remaining constant for ~200 m above, the porosity decreases sharply at ~340 mbsf and follows a normal consolidation curve below (Shipboard Scientific Party, 2001a). The porosity decrease at ~340 mbsf is associated with a diagenetic shift from cristobalite to quartz (Shipboard Scientific Party, 2001a), probably due to the alteration of vitric volcanic ash (Tada and Iijima, 1983) and siliceous microfossils. The stepwise porosity reduction at the cristobalite–quartz transition at Site 1173 mimics similar sharp porosity reductions across a similar phase transition (opal-CT to quartz) in siliceous rocks (Isaacs et al., 1983). Isaacs et al. (1983) believe that the opal-CT to quartz transition is associated with a reorganization and partial collapse of the sediment fabric that had previously been held open by an opal-CT cementation effect. A similar process could explain the sharp shift in porosity at Site 1173. At Site 1173 the abrupt shift in porosity and density at 320–360 mbsf generates a strong seismic reflection. This reflection cuts upsection across stratigraphy from southeast of Site 1173 northwesterly toward the margin (Fig. F4). Important questions here are, "What is the three-dimensional geometry of this reflector?" and "Does this surface represent an isothermal boundary of the opal-CT to quartz transition?"

The cristobalite to quartz phase transition occurs above the stratigraphic level to which the déollement would project at Site 1173, also at Site 1174, and, arguably, at Site 1177. Thus, the décollement seems to propagate seaward entirely in the apparently stronger, more dewatered portion of the Shikoku Basin deposits and does not jump upsection to the less-dewatered section above 320 mbsf. Key questions raised by this observation are, "What is the real strength difference between the sediments above and below the cristobalite to quartz phase transition?" and "What is its effect on décollement development?"

ISONIC Velocity Data

For the first time in ODP history, LWD sonic velocity data were recorded during Leg 196 using Schlumberger's ISONIC tool. In situ velocity information is a key measurement because velocity is the fundamental link between seismic imaging and geology and because velocity is highly sensitive to stress, limiting the utility of shipboard core sample measurements. ISONIC data were recorded at both Sites 1173 and 808. Owing to the complex signal arrivals and the variety of phases propagating along the tool and borehole, compressional wave traveltime picking and, hence, velocity calculation is not straightforward. Initial traveltime analysis of the waveforms recorded during the leg did not

produce reliable velocity values, although features in the velocity logs broadly correlate with those in the resistivity and density logs. Usable velocity and acoustic impedance results will require detailed waveform analysis to be carried out postcruise.

REFERENCES

Ando, M., 1975. Source mechanisms and tectonic significance of historical earthquakes along the Nankai Trough, Japan. *Tectonophysics,* 27:119–140.

Bray, C.J., and Karig, D.E., 1985. Porosity of sediments in accretionary prisms and some implications for dewatering processes. *J. Geophys. Res.*, 90:768–778.

Carson, B., Suess, E., and Strasser, J.C., 1990. Fluid flow and mass flux determinations at vent sites on the Cascadia margin accretionary prism. *J. Geophys. Res.,* 95:8891–8889.

Fisher, D.M., 1996. Fabrics and veins in the forearc: a record of cyclic fluid flow at depths of <15 km. *In* Bebout, G.E., Scholl, D.W., Kirby, S.H., and Platt, J.P., *Subduction Top to Bottom.* Am. Geophys. Union, Geophys. Monogr., 96:75–89.

Henry, P., Lallemant, S.J., LePichon, X., and Lallemand, S.E., 1989. Fluid venting along Japanese trenches; tectonic context and thermal modeling. *Tectonophysics,* 160:277–292.

Hickman, S., Sibson, R., and Bruhn, R., 1995. Introduction to special section: mechanical involvement of fluids in faulting. *J. Geophys. Res.,* 100B:12,831–12,840.

Hill, I.A., Taira, A., Firth, J.V., et al., 1993. *Proc. ODP, Sci. Results,* 131: College Station, TX (Ocean Drilling Program).

Hills, D.J., Moore, G.F., Bangs, N.L., Gulick, S.S., and Leg 196 Shipboard Scientific Party, 2001. Preliminary results from integration of 2D PSDM and ODP Leg 196 LWD velocity data in the Nankai accretionary prism. *Eos, Trans., Am. Geophys. Union,* 82:F1221.

Isaacs, C.M., Pisciotto, K.A., and Garrison, R.E., 1983. Facies and diagenesis of the Miocene Monterey Formation, California: a summary. *In* Iijima, A., Hein, J.R., and Siever, R. (Eds.), *Siliceous Deposits in the Pacific Region.* Dev. Sedimentol. Ser., U.S. Geol. Surv., 36:247–282.

Kanamori, H., 1986. Rupture process of subduction-zone earthquakes. *Annu. Rev. Earth Planet. Sci.,* 14:293–322.

Kastner, M., Elderfield, H., Jenkins, W.J., Gieskes, J.M., and Gamo, T., 1993. Geochemical and isotopic evidence for fluid flow in the western Naikai subduction zone, Japan. *In* Hill, I.A., Taira, A., Firth, J.V., et al., *Proc. ODP, Sci. Results,* 131: College Station, TX (Ocean Drilling Program), 397–413.

Kastner, M., Elderfield, H., and Martin, J.B., 1991. Fluids in convergent margins: what do we know about their composition, origin, role in diagenesis and importance for oceanic chemical fluxes? *Philos. Trans. of the R. S. London A,* 335:243–259.

Kodaira, S., Takahashi, N., Park, J., Mochizuki, K., Shinohara, M., and Kimura, S., 2000. Western Nankai Trough seismogenic zone: results from a wide-angle ocean bottom seismic survey. *J. Geophys. Res.,* 105:5887–5905.

Lallemant, S., Byrne, T., Maltman, A.J., Karig, D.E., and Henry, P., 1993. Stress tensors at the toe of the Nankai accretonary prism: an application of inverse methods to slickenlined faults. *In* Hill, I.A., Taira, A., Firth, J.V., et al., *Proc. ODP Sci. Results,* 131: College Station, TX (Ocean Drilling Program), 103–122.

Mazzotti, S., LePichon, X., Henry, P., and Miyazaki, S., 2000. Full interseismic locking of the Nankai and Japan-West Kuril subduction zones: an analysis of uniform elastic strain accumulation in Japan constrained by permanent GPS. *J. Geophys. Res.,* 105:13159–13177.

Moore, G.F., Taira, A., Bangs, N.L., Kuramoto, S., Shipley, T.H., Alex, C.M., Gulick, S.S., Hills, D.J., Ike, T., Ito, S., Leslie, S.C., McCutcheon, A.J., Mochizuki, K., Morita, S., Nakamura, Y., Park, J.-O., Taylor, B.L., Yagi, H., and Zhao, Z., 2001. Data report: Structural setting of the Leg 190 Muroto Transect. *In* Moore, G.F., Taira, A., Klaus, A., et al., *Proc. ODP, Init. Repts.,* 190, 1–14 [CD-ROM]. Available from: Ocean Drilling Program, Texas A&M University, College Station TX 77845-9547, USA.

Moore, G.F., Taira, A., Klaus, A., et al., 2001. *Proc. ODP, Init. Repts.,* 190 [CD-ROM]. Available from: Ocean Drilling Program, Texas A&M University, College Station TX 77845-9547, USA.

Moore, J.C., and Vrolijk, P., 1992. Fluids in accretionary prisms. *Rev. Geophys.,* 30:113–135.

Moores, E.M., and Twiss, R.J., 1995. *Tectonics:* New York (W.H. Freeman and Company).

Morgan, J.K., and Karig, D.E., 1995. Kinematics and a balanced and restored cross-section across the toe of the eastern Nankai accretionary prism. *J. Struct. Geol.,* 17:31–45.

Okino, K., Ohara, Y., Kasuga, S., and Kato, Y., 1999. The Philippine Sea: new survey results reveal the structure and history of marginal basins. *Geophys. Res. Lett.,* 26:2287–2290.

Park, J.-O., Tsuru, T., Kodaira, S., Nakanishi, A., Miura, S., Kaneda, Y., and Kono, Y., 2000. Out-of-sequence thrust faults developed in the coseismic slip zone of the 1946 Nankai earthquake (Mw = 8.2) off Shikoku, southwest Japan. *Geophys. Res. Lett.,* 27:1033–1036.

Plank, T., Stern, R., and Morris, J., 1998. The subduction factory science plan, MARGINS Program. *Nat. Sci. Found.* <http://www.soest.hawaii.edu/margins/SubFac.html>

Seno, T., Stein, S., and Gripp, A.E., 1993. A model for the motion of the Philippine Sea plate consistent with NUVEL-1 and geological data. *J. Geophys. Res.,* 98:17941–17948.

Shipboard Scientific Party, 1991. Site 808. *In* Taira, A., Hill, I., Firth, J., et al., *Proc. ODP, Init. Repts.,* 131: College Station, TX (Ocean Drilling Program), 71–269.

————, 2001a. Site 1173. *In* Moore, G.F., Taira, A., Klaus, A., et al., *Proc. ODP, Init. Repts.,* 190, 1–147 [CD-ROM]. Available from: Ocean Drilling Program, Texas A&M University, College Station TX 77845-9547, USA.

————, 2001b. Site 1174. *In* Moore, G., Taira, A., Klaus, A., et al., *Proc. ODP, Init. Repts.,* 190, 1–149 [CD-ROM]. Available from: Ocean Drilling Program, Texas A&M University, College Station TX 77845-9547, USA.

Suess, E., and Whiticar, M.J., 1989. Methane-derived CO_2 in pore fluids expelled from the Oregon subduction zone. *Palaeogeogr., Palaeoclimatol., Palaeoecol.,* 71:119–136.

Tada, R., and Iijima, A., 1983. Identification of mixtures of opaline silica phases and its implication for silica diagenesis. *In* Iijima A., Hein, J.R., and Siever, R. (Eds.), *Siliceous Deposits in the Pacific Region.* Dev. Sedimentol. Ser., U.S. Geol. Surv., 229–245.

Taira, A., Katto, J., Tashiro, M., Okamura, M., and Kodama, K., 1988. The Shimanto Belt in Shikoku, Japan: evolution of a Cretaceous to Miocene accretionary prism. *Mod. Geol.,* 12:5–46.

Vrolijk, P., Fisher, A., and Gieskes, J., 1991. Geochemical and geothermal evidence for fluid migration in the Barbados accretionary prism (ODP Leg 110). *Geophys. Res. Lett.,* 18:947–950.

Wang, K., Hyndman, R.D., and Yamano, M., 1995. Thermal regime of the Southwest Japan subduction zone: effects of age history of the subducting plate. *Tectonophysics,* 248:53–69.

Yamano, M., Foucher, J.-P., Kinoshita, M., Fisher, A., Hyndman, R.D., and ODP Leg 131 Shipboard Scientific Party, 1992. Heat flow and fluid flow regime in the western Nankai accretionary prism. *Earth Planet. Sci. Lett.,* 109:451–462.

Figure F1. Map showing locations of Leg 190 and 196 sites. The red box outlines the location of the three-dimensional seismic survey. Yellow numbers indicate sites revisited during Leg 196. Depth contours are in kilometers.

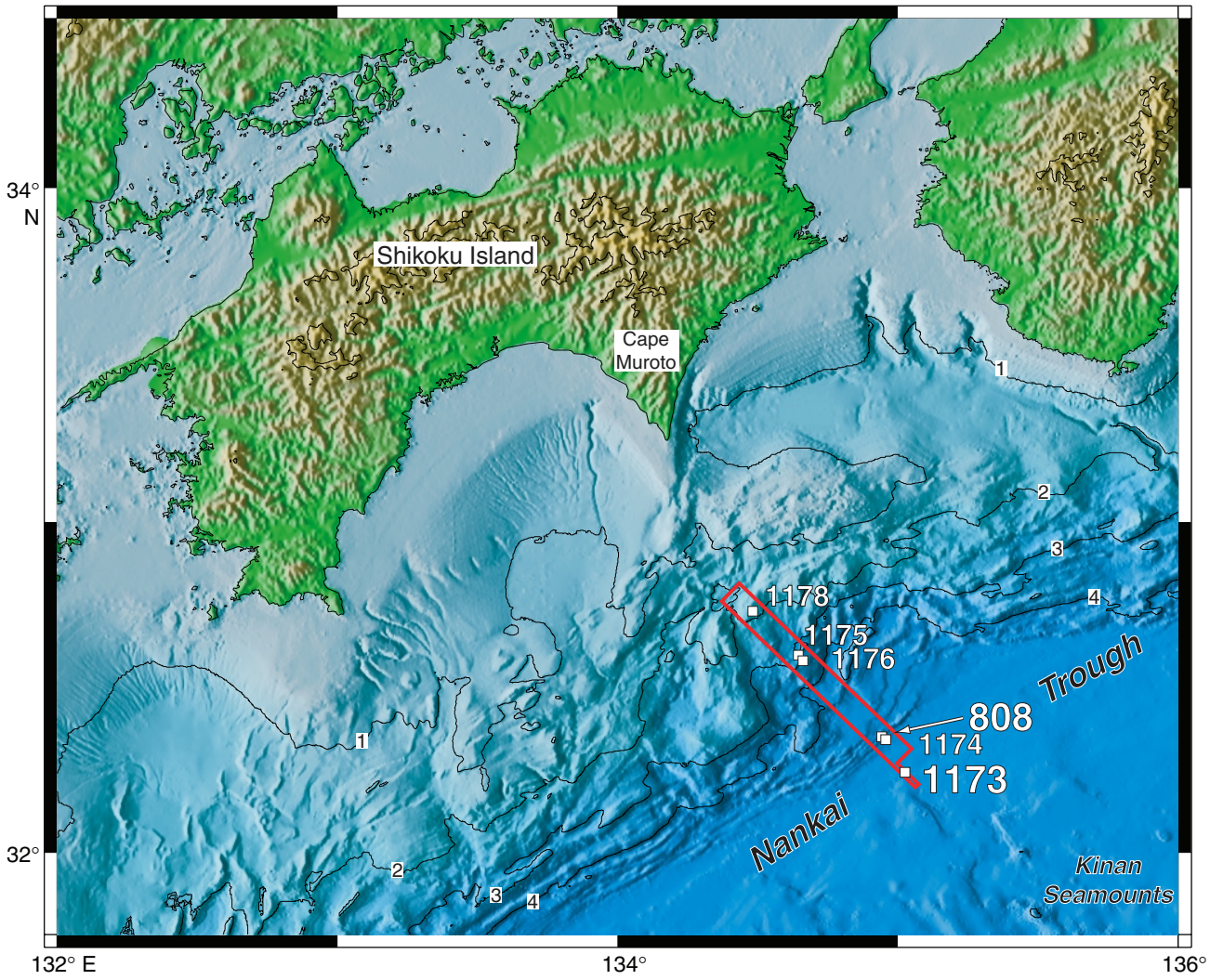

Figure F2. Generalized depth section showing site locations and major structural features and provinces. This drawing is based on seismic reflection data from Hills et al. (2001). VE = vertical exaggeration.

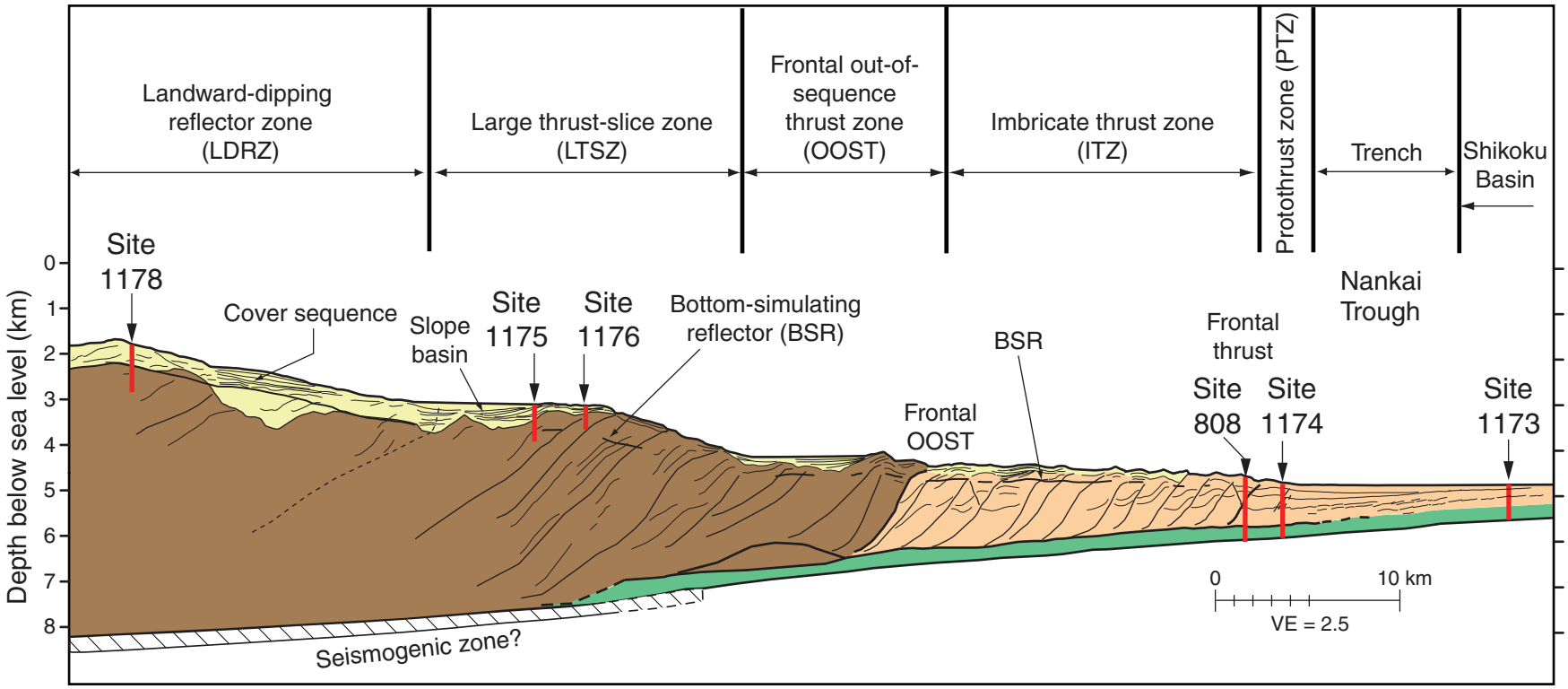

Figure F3. Seismic time section across Leg 196 Sites 1173 and 808 showing the transition from the Shikoku Basin to the imbricate thrust zone. The section is composed of a northwest-trending segment of seismic line 215 through Site 1173, with a diagonal transition to line 281 that passes near Sites 1174 and 808. CDP = common depth point, VE = vertical exaggeration.

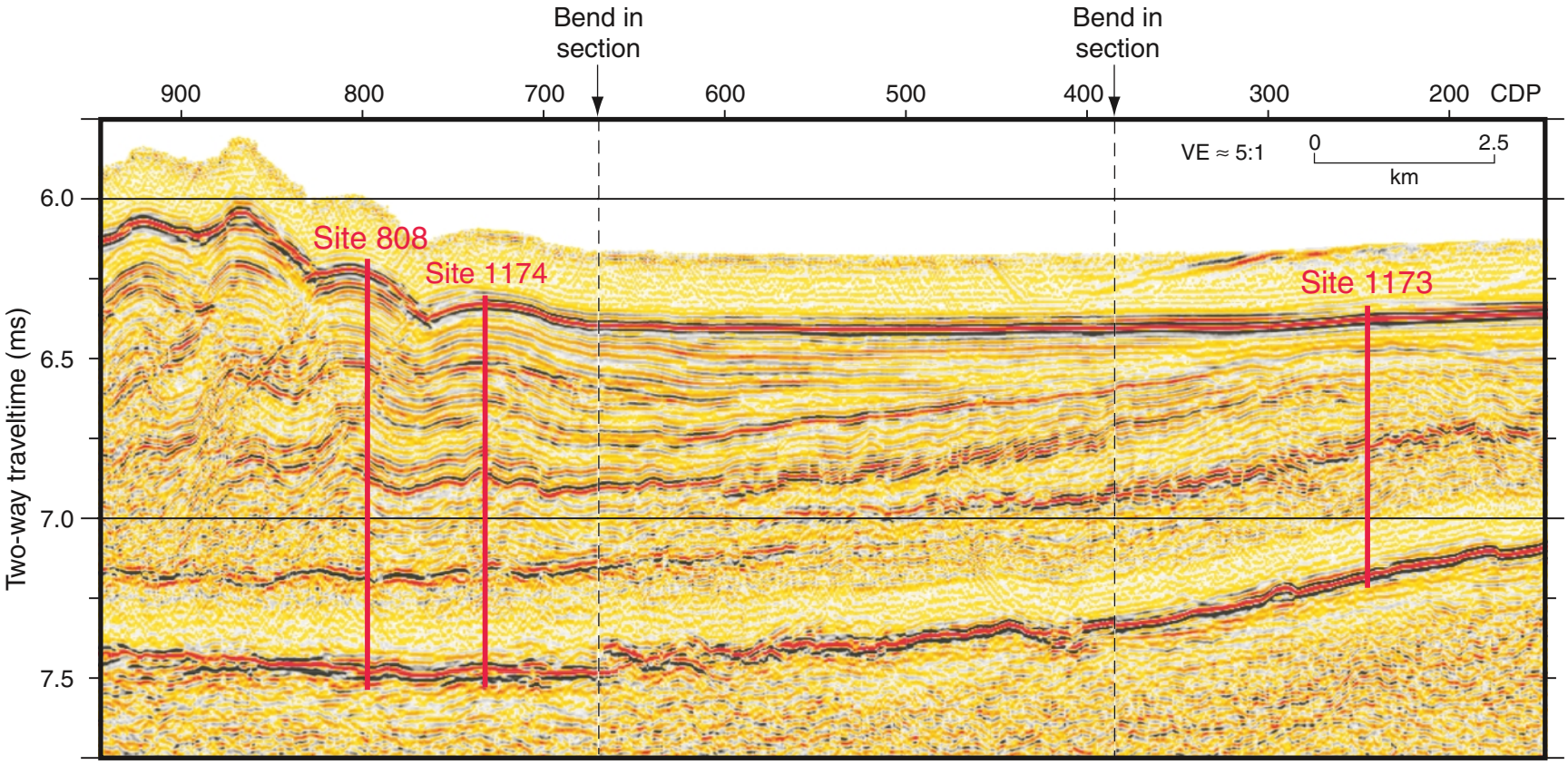

Figure F4. Seismic depth section across Sites 1173, 1174, and 808 (Hills et al., 2001). The section is composed of a northwest-trending segment of seismic line 215 through Site 1173, with a diagonal transition to line 281 that passes near Sites 1174 and 808. CDP = common depth point, VE = vertical exaggeration.

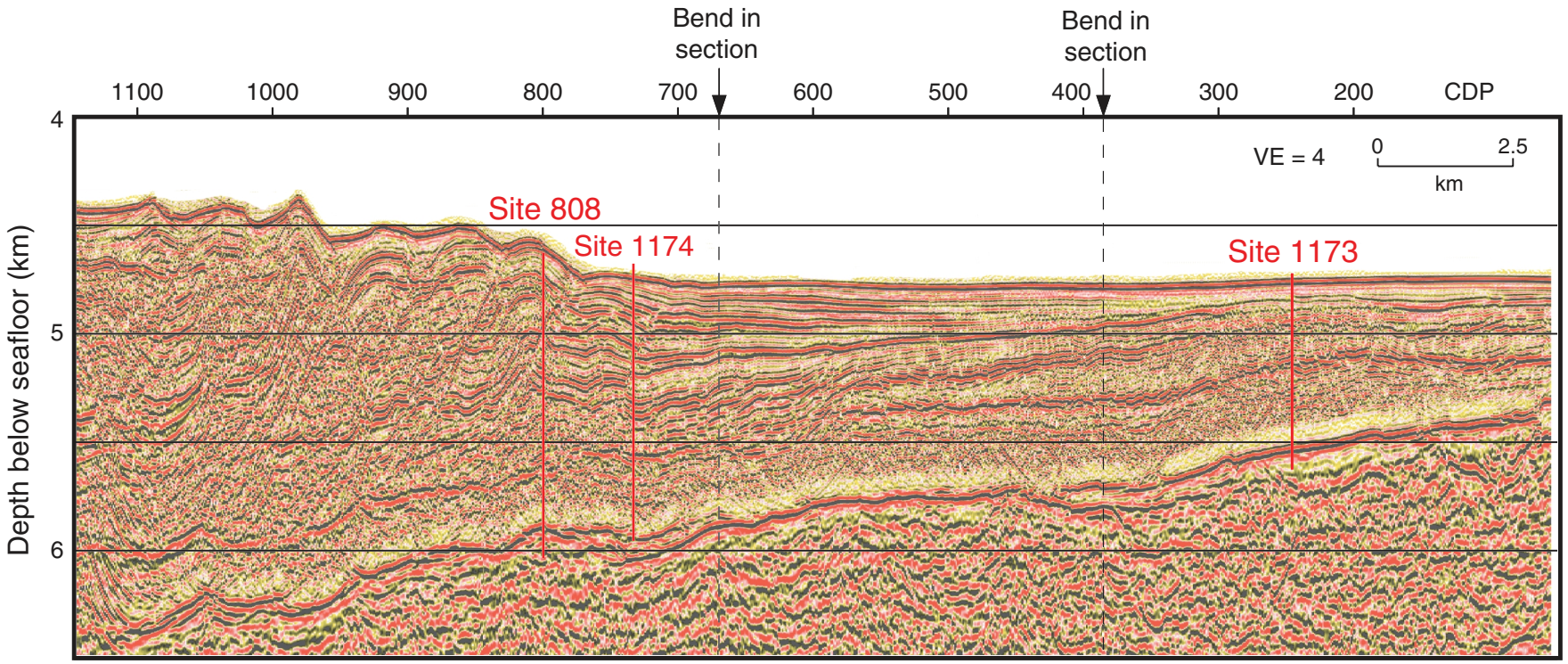

Figure F5. Composite seismic section through Leg 196 drill sites. See map (upper right) for location and geometry of the composite construction. These data were obtained as part of a three-dimensional (3-D) seismic reflection volume acquired during a 1999 *Ewing* cruise. The top section is a two-dimensional prestack depth-migrated version of a section from the 3-D data volume. The bottom section shows the same data converted to time. This version of the data is from Hills et al. (2001). CMP = common midpoint, VE = vertical exaggeration. (This figure is also available in an **oversized format**.)

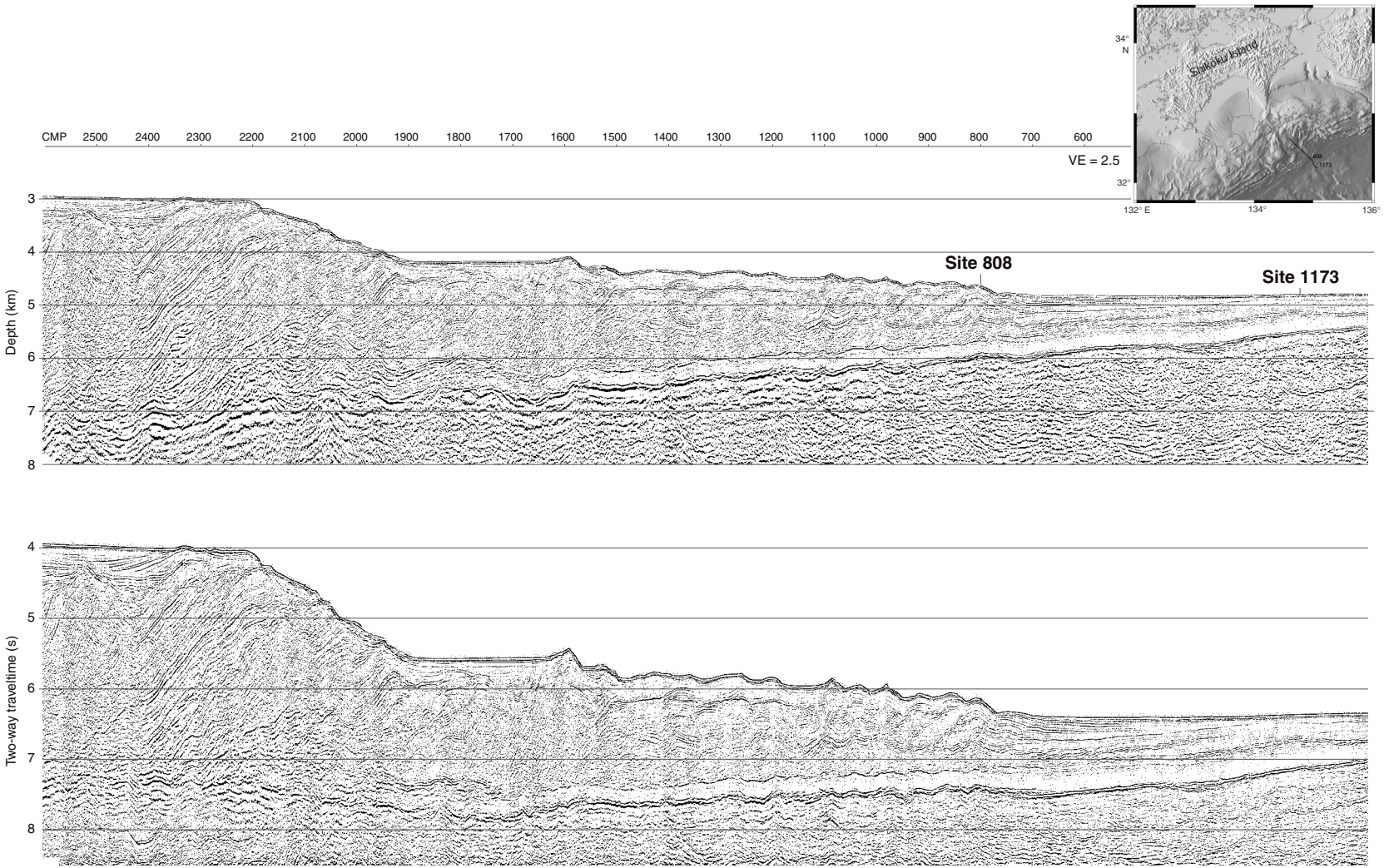

Figure F6. Site 1173 summary diagram showing combined results of Legs 190 and 196. From left to right: depth-converted seismic reflection data, core recovery, core-based lithology and facies interpretation, bedding dip, pore water geochemistry, temperature-depth gradient, wireline and log resistivity, clay mineral content (solid circles) and gamma ray log, core and log density, core and log porosity (computed from the density log using core grain density values), log units, and a schematic diagram of the Advanced CORK (ACORK). CDP = common depth point, RAB = resistivity at the bit, SFLU = spherically focused resistivity measurement, XRD = X-ray diffraction. (This figure is also available in an **oversized format.**) (Continued on next page.)

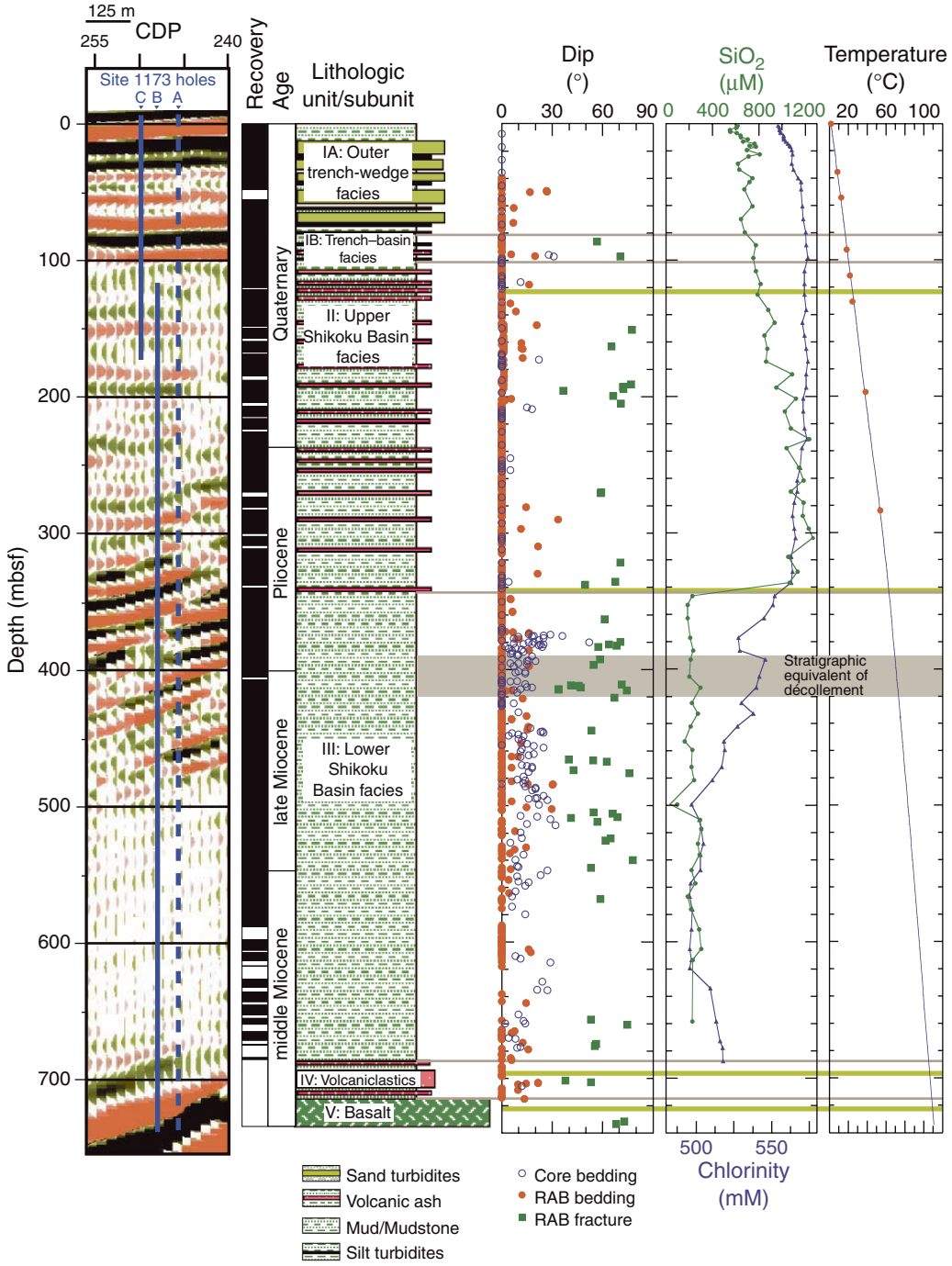

Figure F6 (continued).

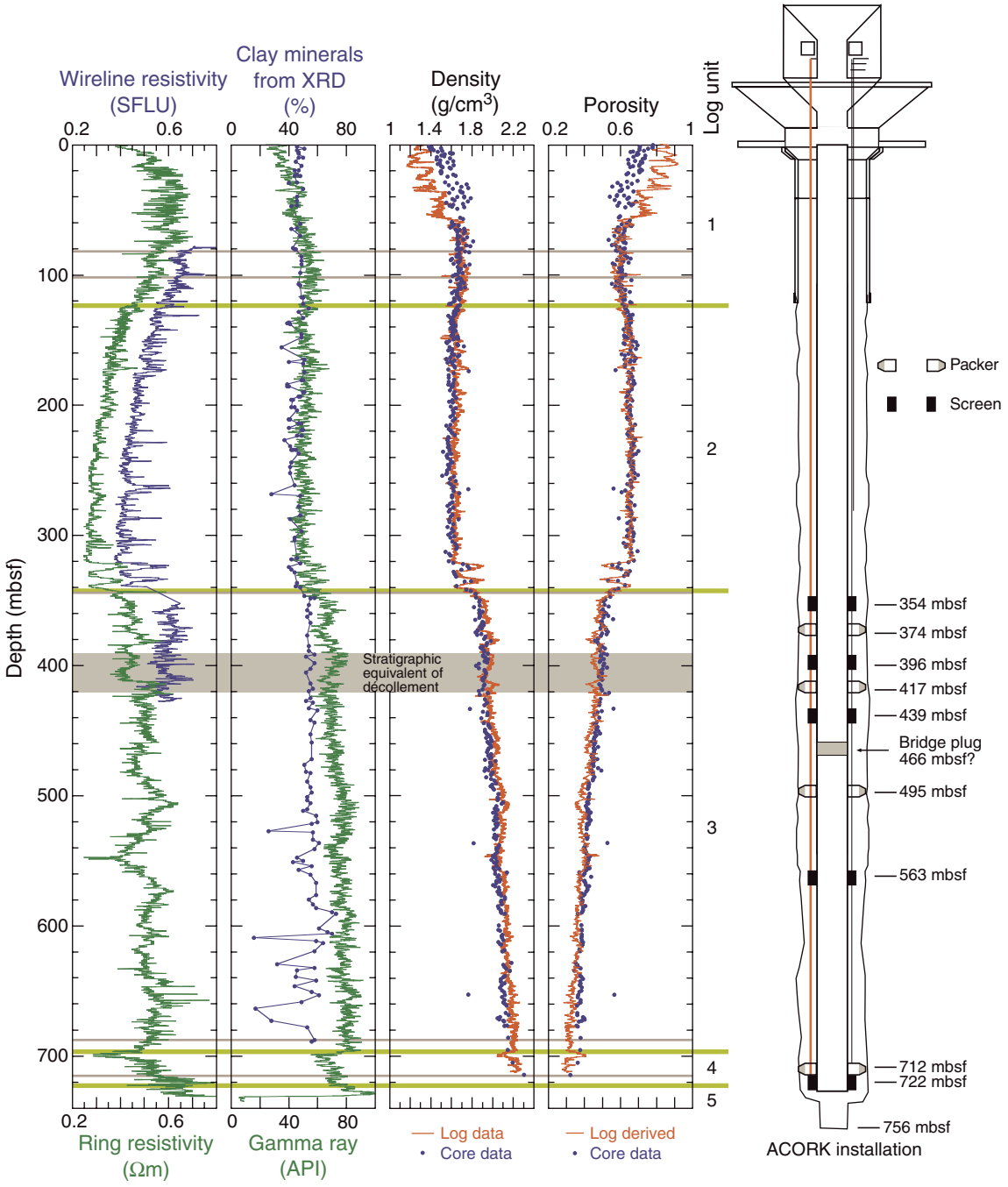

Figure F7. Site 808 summary diagram showing combined results of Legs 131 and 196. From left to right: depth-converted seismic reflection data, core-based facies interpretation, core recovery, core-based lithologic units and lithology, log gamma ray, core and log density, core and log porosity (computed from the density log using core grain density values), pore water chlorinity, fracture dip from resistivity-at-the-bit (RAB) images, core *P*-wave velocity, log resistivity, log units, and a schematic diagram of the Advanced CORK (ACORK). CDP = common depth point, MWD = measurement while drilling. (This figure is also available in an **oversized format.**) (Continued on next page.)

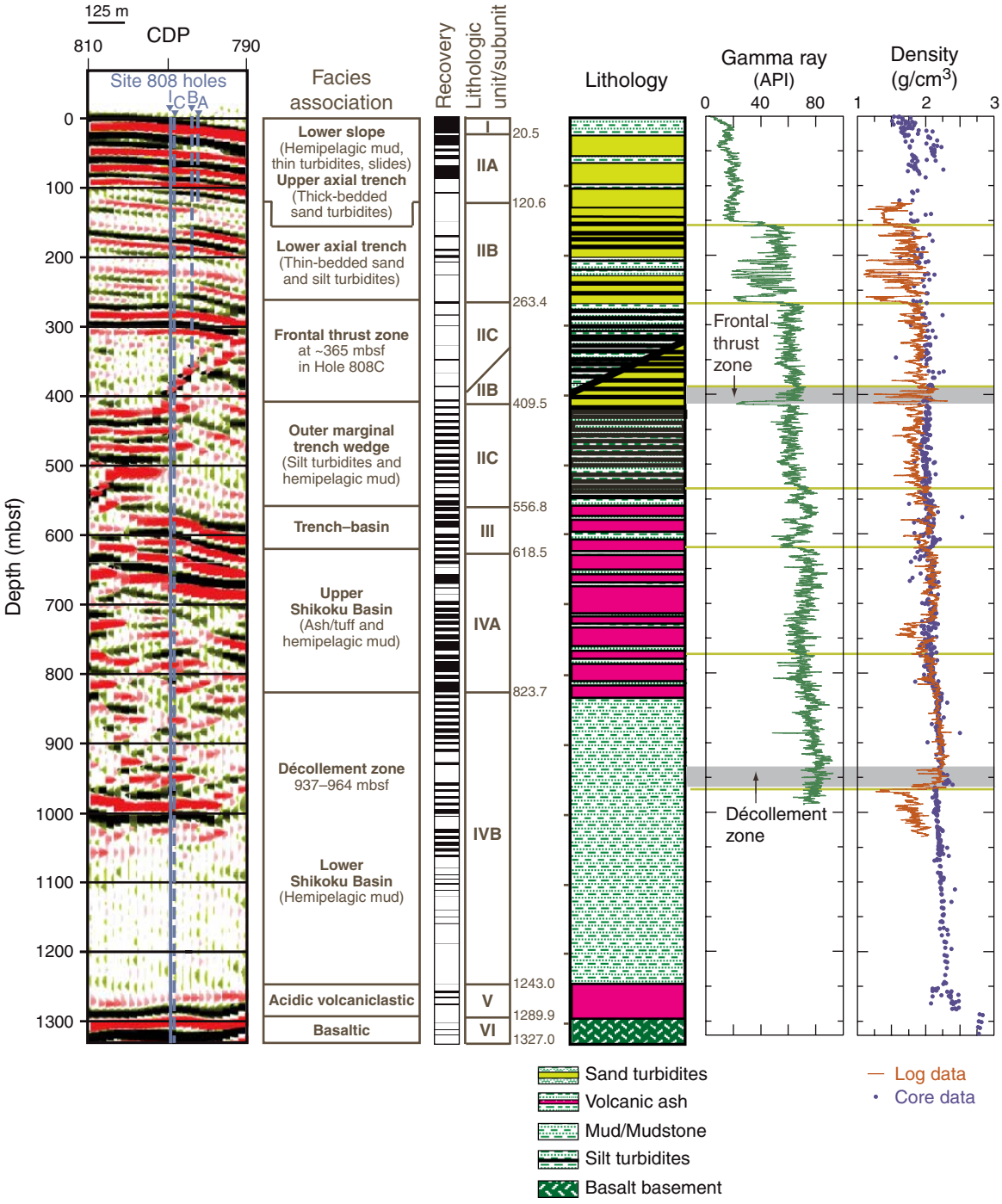

Figure F7 (continued).

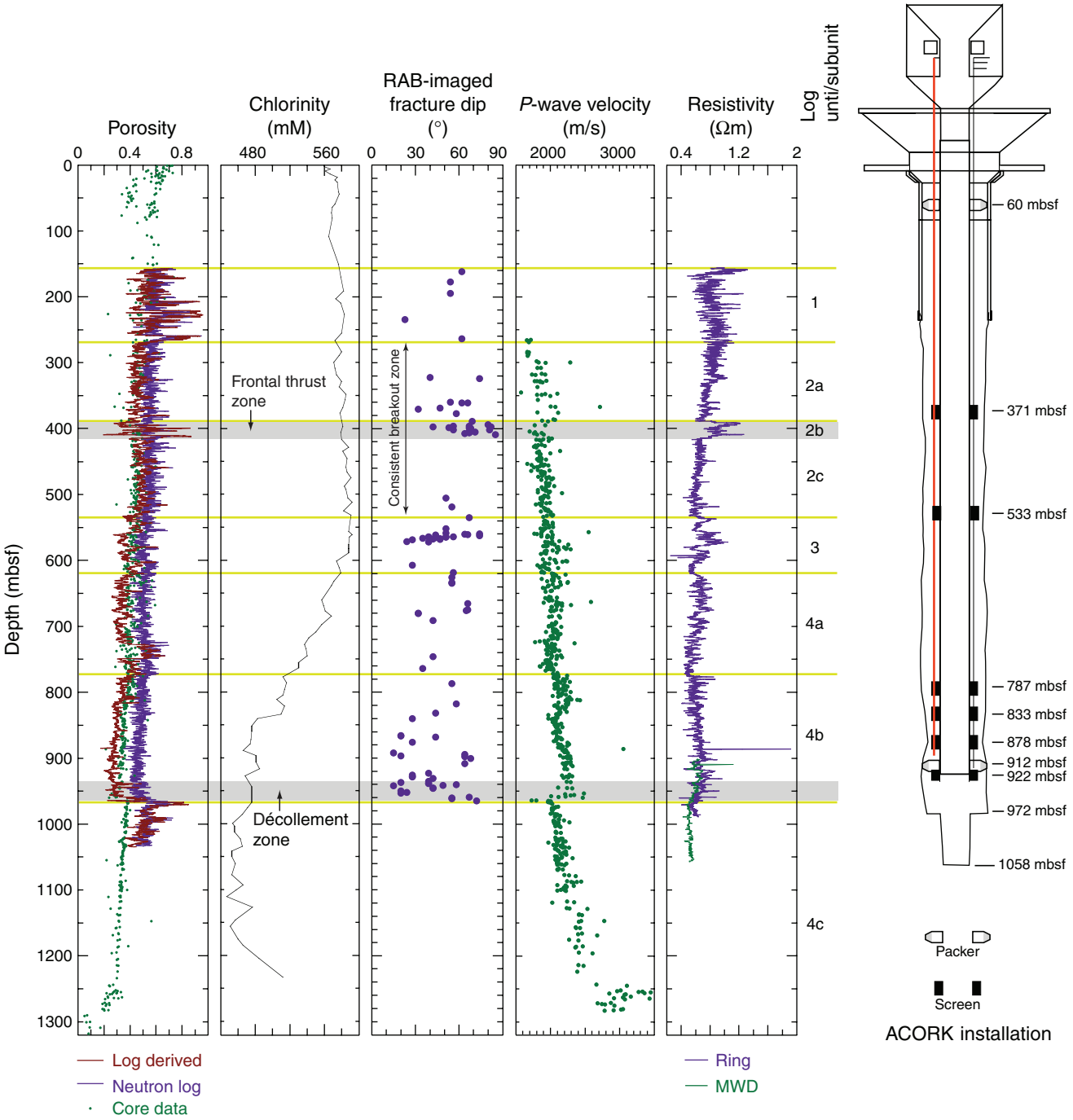

Figure F8. Resistivity-at-the-bit image of Hole 808I showing all interpreted fractures. Fractures are separated into conductive (blue) and resistive (red) fractures. Tadpoles show fractures as dip direction with respect to north and dip (0°–90°). Deformation intensifies significantly at the frontal thrust (389–414 mbsf), a fractured interval correlated with Leg 131 Site 808 core analysis (559–574 mbsf), and the décollement zone (~950 mbsf). The interval of continuous strong borehole breakouts is labeled between ~270 and ~530 mbsf, coincident with log Unit 2 and bracketing the frontal thrust zone. Fracture orientations are dominantly northeast-southwest (northwest-southeast dip directions) within the frontal thrust zone and 560-mbsf fractured interval but are more variably oriented with depth. A north-south fracture orientation (east-west dip direction) is dominant within the décollement zone.

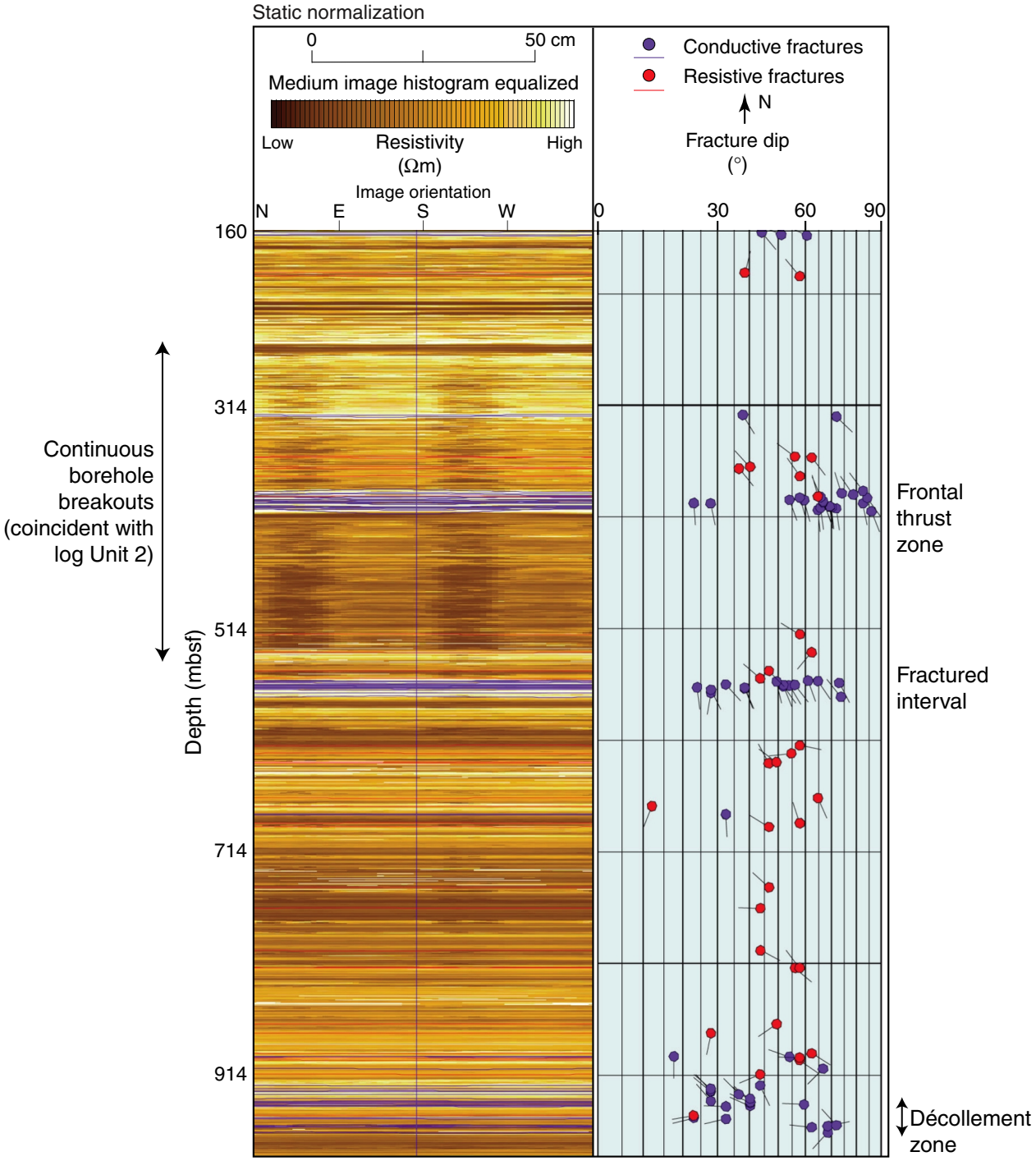

Figure F9. Hole 808I breakouts (dark low-resistivity parallel lines) at 460–505 mbsf interpreted from resistivity-at-the-bit images at 1-in (shallow), 3-in (medium), and 5-in (deep) penetration from the borehole. This image is ~100 m below the frontal thrust zone, close to the base of log Unit 2. The breakouts indicate that the orientation of the minimum horizontal compressive stress (σ_2) is ~northeast-southwest, which is in good agreement with the plate convergence vector of ~310°–315° aligned with the maximum compressive stress, σ_1 (90° to σ_2).

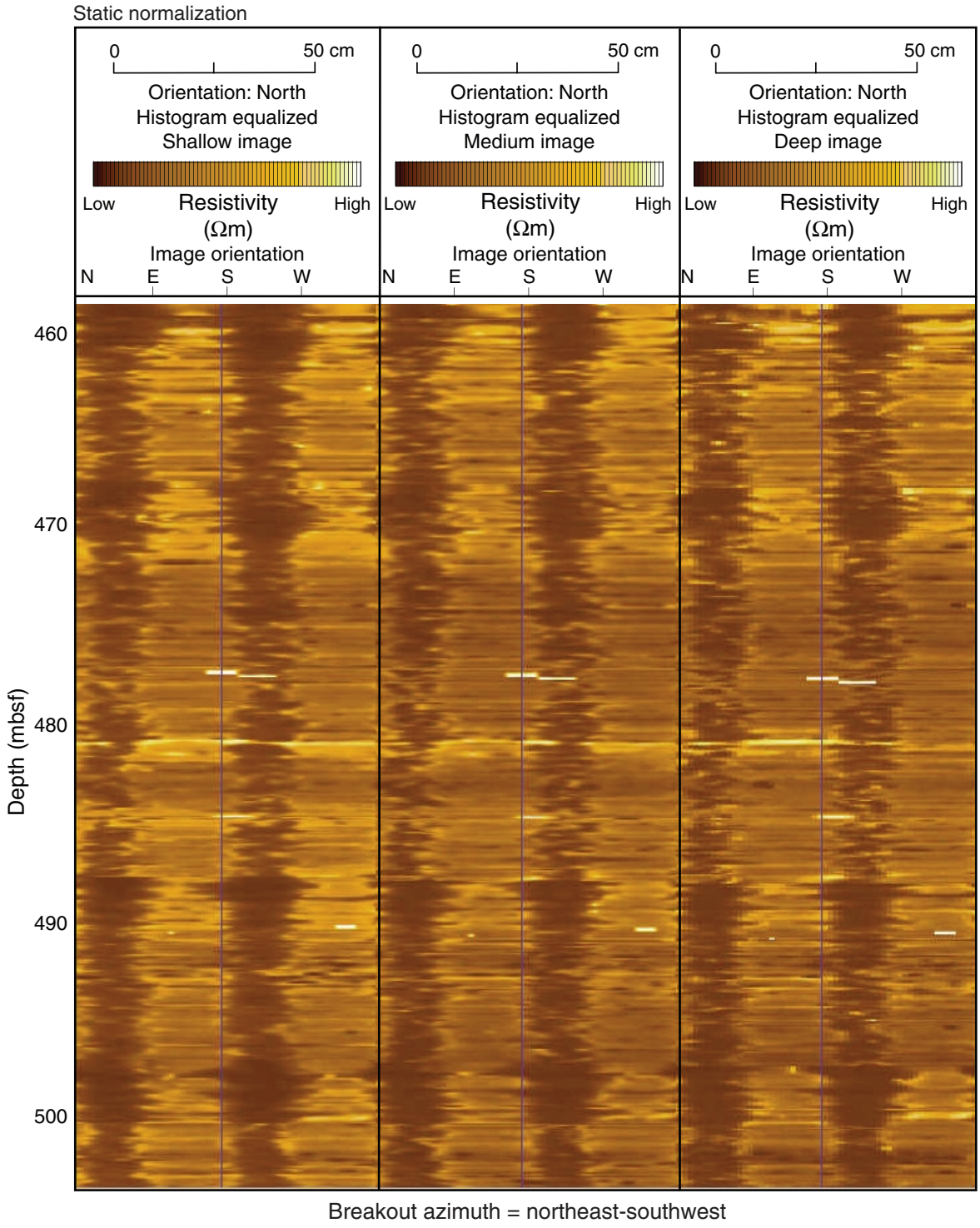

Table T1. Operations summary, Leg 196. (See table notes. Continued on next page.)

Hole 1173B
Latitude: 32°14.6831′N
Longitude: 135°01.4845′E
Seafloor (drill pipe measurement from rig floor, mbrf): 4801.9
Distance between rig floor and sea level (m): 10.8
Water depth (drill pipe measurement from sea level, m): 4791.1

Hole 1173C
Latitude: 32°14.6978′N
Longitude: 135°01.4612′E
Seafloor (drill pipe measurement from rig floor, mbrf): 4801.9
Distance between rig floor and sea level (m): 10.8
Water depth (drill pipe measurement from sea level, m): 4791.1

Operation	Start		End		Depth (mbsf)		Drilled (mbsf)	Time on hole		Comments
	Date (2001)	Time (local)	Date (2001)	Time (local)	Top	Bottom		Hours	Days	
196-1173B:										
Install reentry cone and 20-in casing	10 May	0224	13 May	2315	0	124.2	124.2	88.5	3.69	20-in casing shoe at 120.6 mbsf; includes 43 hr due to reentry cone loss.
LWD	13 May	2315	17 May	2135	124.2	737.1	612.9	94.3	3.93	Includes 24 hr spent evading tropical storm.
Open 9⅞-in LWD hole to 17½ in for ACORK	23 May	1910	2 Jun	0230	124.2	735.1	610.9	79.3	3.31	17½-in hole extends to 732.1 mbsf.
Assemble and drill in ACORK	2 Jun	0230	10 Jun	0445	—	—	—	194.2	8.09	ACORK extends from 0 to 727.10 mbsf; includes 58-hr DP transit back to site.
RCB core below ACORK: Open basement hydrologic system to deepest monitoring zone	10 Jun	0445	12 Jun	1615	737.1	756.6	19.5	59.5	2.48	Three cores; 19.5 m cored; 5.19 m recovered (27%).
Install bridge plug inside ACORK	12 Jun	1615	14 Jun	0000	—	—	—	31.7	1.32	Bridge plug set at 466 mbsf; drill pipe broke off at ACORK head.
Conduct camera survey of ACORK	29 Jun	0400	29 Jun	2215	—	—	—	18.3	0.76	
					Totals for Hole 1173B:		1367.5	565.8	23.58	
196-1173C:										
LWD	17 May	2135	18 May	1655	0	175.0	175.0	19.4	0.81	
					Totals for Hole 1173C:		175.0	19.4	0.81	
					Totals for Site 1173:		1542.5	585.2	24.39	

Table T1 (continued).

Hole 808H
Latitude: 32°21.2142′N
Longitude: 134°56.7009′E
Seafloor (drill pipe measurement from rig floor, mbrf): 4686.0
Distance between rig floor and sea level (m): 10.9
Water depth (drill pipe measurement from sea level, m): 4675.1

Hole 808I
Latitude: 32°21.2145′N
Longitude: 134°56.7003′E
Seafloor (drill pipe measurement from rig floor, mbrf): 4686.0
Distance between rig floor and sea level (m): 10.9
Water depth (drill pipe measurement from sea level, m): 4675.1

Operation	Start		End		Depth (mbsf)		Drilled (mbsf)	Time on hole		Comments
	Date (2001)	Time (local)	Date (2001)	Time (local)	Top	Bottom		Hours	Days	
196-808H:										
Install reentry cone and 20-in casing	18 May	1937	20 May	1910	0	126.7	126.7	47.5	1.98	Mud motor failed; pulled out of hole; hole abandoned.
					Totals for Hole 808H:		126.7	47.5	1.98	
196-808I:										
Install reentry cone and 20-in casing	20 May	1910	22 May	1130	0	160.1	160.1	40.3	1.68	20-in casing shoe at 156.6 mbsf.
LWD	22 May	1130	27 May	1710	160.1	1057.6	897.4	125.7	5.24	Unable to penetrate past 1057.6 mbsf.
Open 9⅞-in LWD hole to 17½ in for ACORK	14 Jun	0130	18 Jun	1555	160.1	975.3	815.2	110.4	4.60	
Assemble and drill in ACORK	18 Jun	1555	28 Jun	1945	—	—	—	243.8	10.16	964-m-long ACORK could only be drilled in to 927 mbsf; time on hole includes 17-hr DP transit back to site.
					Totals for Hole 808I:		1872.7	520.2	21.68	
					Totals for Site 808:		1999.4	567.7	23.66	
					Totals for Leg 196:		3541.9	1152.9	48.05	

Notes: LWD = logging while drilling, ACORK = Advanced CORK, RCB = rotary core barrel. DP = dynamic positioning. — = not applicable.